Theoretical and Applied Fracture Mechanics 114 (2021) 103020

Contents lists available at ScienceDirect

Theoretical and Applied Fracture Mechanics

journal homepage: www.elsevier.com/locate/tafmec

Large deformation near a crack tip in a fiber-reinforced neo-Hookean sheet with discrete and continuous distributions of fiber orientations

Luca Di Stasio *, Yin Liu, Brian Moran

Division of Physical Sciences and Engineering, King Abdullah University of Science and Technology (KAUST), Thuwal 23955-6900, Saudi Arabia

ARTICLE INFO

Keywords:
Finite elasticity
Neo-Hookean
Fiber orientation distribution
Crack tip fields
Asymptotic analysis
Finite element analysis (FEA)

ABSTRACT

We consider crack tip deformations under plane stress conditions of a Neo-Hookean sheet reinforced by Neo-Hookean fibers, whose orientation and elastic properties are described by discrete and continuous spatial distributions. The mechanical behavior of the composite is described in terms of the first and fourth invariant of the right Cauchy-Green tensor following Guo et al. [1–3]. The crack tip integrals developed in Liu and Moran [4,5] are used to determine the coefficients of the crack tip asymptotic expansion. The *von Mises* distribution of orientation is analyzed. The existence of a regime of isotropic behavior, which we call *asymptotic isotropy*, in the region of dominance of the asymptotic fields is established for certain combinations of fiber orientations. Finally, the possibility to construct an *asymptotic universal one-to-one mapping* between anisotropic and isotropic Neo-Hookean plane stress response at the crack tip is discussed.

1. Introduction

A large class of both biological and synthetic bioinspired soft materials can be modeled as composed of a hyperelastic matrix reinforced by one or more families of hyperelastic fibers. Each family of fibers is characterized by their specific elastic properties and an orientation in space, and the overall variation in elastic properties and orientations is expressed in terms of discrete or continuous distributions. We thus refer to this class of materials as hyperelastic materials reinforced by a distribution of fibers. Examples are numerous: articular cartilage [6], human cornea [7], aneurysms [8], human brain arteries [9], muscle tissue [10], the aorta [11], aortic heart valves [12], hydrogels [13], scaffolding materials to grow load-bearing soft tissues [14], ink-printed hydrogels reinforced by cellulose fibrils [15].

Focusing on the mechanical response of arterial layers, the importance of the presence of distributions of fibers in soft materials is emphasized in [16]. In the latter, the authors include the effect of the distributed fiber orientations through a generalized structure tensor in the framework of anisotropic large-deformation elasticity. By means of numerical experiments, they show that the mechanical response of the soft-composite is strongly dependent of the fiber distribution. A highly dispersed distribution of orientations translates into a stiffer material less dependent on the main direction of alignment of the fibers, whereas a distribution concentrated around the main direction causes a highly direction-dependent response. They furthermore observe that, in the case of a single fiber orientation, fibers undergo large rotations before carrying load to align with the direction of the applied load. They thus conclude that the study of ideally aligned fibers, i.e. all parallel to one direction, is not sufficient to predict the mechanical response of fiber-reinforced soft materials. In [16], the authors adopt a continuum mechanics approach and use the strain-energy superposition assumption. Based on the volumetric-distortional decomposition of [17,18], the strain-energy superposition assumption allows the additive split of the strain energy into a purely volumetric term and a purely distortional term [19] and it is valid for incompressible and nearly-incompressible materials [20]. In the case of fiber-reinforced soft composites, the matrix may be considered as the driver of volumetric deformations whereas fibers are responsible for the isochoric distortional part of the deformation. Thus, the contribution to the strain energy density of the two phases can be additively split by identifying the matrix contribution with the volumetric term and the fiber contribution with the distortial term of the volumetric-distortional decomposition [6,21]. In the presence of multiple families of fibers located in a finite and discrete set of orientations and properties, the contributions of each family of fibers (meant as a set of fibers with one specific orientation and the same set of mechanical properties) are summed up to provide the distortional part of the strain-energy density [22]. In the case of a continuous distribution of orientations and/or mechanical properties, the finite sum becomes a

* Corresponding author.
E-mail addresses: luca.distasio@kaust.edu.sa (L. Di Stasio), yin.liu@kaust.edu.sa (Y. Liu), brian.moran@kaust.edu.sa (B. Moran).

https://doi.org/10.1016/j.tafmec.2021.103020
Received 15 February 2021; Received in revised form 11 May 2021; Accepted 13 May 2021
Available online 19 May 2021

distribution-weighted integral [6,16,21,23]. Further details on the continuum mechanics approach to modeling fiber-reinforced soft materials with discrete or continuous distribution of orientations or properties can be found in the reviews of [24,25]. Efforts at modeling the failure behavior have proposed a number of approaches, namely limiting failure criteria [26], softening models [27], micro-structural damage mechanisms [28,29], cohesive surfaces [30], internal damage variables [31,32], permanent deformations [33], statistical approaches [34], bond kinetics [35], phase field modeling [36] (see [37] for a thorough review on the subject).

It appears however that the analysis of the behavior of the elastic fields at the crack tip remains unaddressed. In [4], a set of crack tip contour integrals is presented to evaluate the parameters determining the stress and deformation fields at the crack tip in an isotropic hyperelastic material under conditions of plane stress or plane strain. The integrals are then extended in [5] to anisotropic fiber-reinforced soft materials with fibers oriented in one or two directions. Building upon this previous work, the crack tip contour integrals approach is applied in this paper to the analysis of the crack tip large deformation fields in Neo-Hookean sheets reinforced by discrete and continuous distributions of fibers under conditions of plane stress.

This paper is organized as follows. In Section 2, the governing equations of a Neo-Hookean matrix reinforced by discrete and continuous distributions of fibers are introduced for general 3D deformation fields. The model is then restricted to plane stress conditions and its main equations are provided in Section 3. The asymptotic boundary value problem and its solution are introduced in Section 4. Section 5 briefly introduces the crack tip integrals used for the evaluation of the coefficients of the asymptotic expansion derived in Section 4. Numerical results for discrete and continuous distributions of fibers are presented and analyzed in Section 6. Conclusions are finally discussed in Section 7.

2. Governing equations

In the presence of multiple families of fibers, their properties and orientation are described by a distribution function $f(\mathbf{a}_0,\kappa)$. In general, for a given family of fibers the vector

$$\mathbf{a}_0 = \sin\phi\cos\psi\mathbf{e}_1 + \sin\phi\sin\psi\mathbf{e}_2 + \cos\phi\mathbf{e}_3 \tag{1}$$

represents the fiber orientation in the material reference (undeformed) configuration in a three-dimensional space spanned by the unit vectors e_1, e_2, e_3 using the spherical coordinates ϕ and θ (see Fig. 1). On the other hand, the parameter κ in the distribution function $f(\mathbf{a}_0,\kappa)$ represents the ratio of fiber to matrix shear moduli such that $\mu_f = \kappa\mu$ where μ is the matrix shear modulus.

When considered transversely isotropic, the strain energy density function W (per unit of undeformed volume) of fiber-reinforced hyperlastic materials is, in general, a function of the first five invariants I_1, I_2, I_3, I_4, I_5 of the right Cauchy-Green tensor $\mathbf{C} = \mathbf{F}^T\mathbf{F}$ [38]. $\mathbf{F}$ represents the deformation gradient whose components are given by $F_{ij} = \frac{\partial y_i}{\partial x_j}$, where x_j and y_i denote the coordinates respectively in the undeformed and deformed configuration. The first three invariants do not depend on fiber properties and orientation and can be expressed as

$$I_1 = tr\mathbf{C}\ \ I_2 = \frac{1}{2}\left[(tr\mathbf{C})^2 - tr\mathbf{C}^2\right]\ \ I_3 = det\mathbf{C}, \tag{2}$$

or, in terms of the three principal stretches $\lambda_1, \lambda_2, \lambda_3$ as

$$I_1 = \lambda_1^2 + \lambda_2^2 + \lambda_3^2\ \ I_2 = \lambda_1^2\lambda_2^2 + \lambda_2^2\lambda_3^2 + \lambda_3^2\lambda_1^2\ \ I_3 = \lambda_1^2\lambda_2^2\lambda_3^2. \tag{3}$$

On the other hand, the fourth and fifth invariant depend on fiber properties and orientation and can be represented as

$$I_4 = \mathbf{a}_0^T\mathbf{C}\mathbf{a}_0\ \ I_5 = \mathbf{a}_0^T\mathbf{C}^2\mathbf{a}_0. \tag{4}$$

The functional form of the distribution function is such that

$$\frac{1}{4\pi}\int_\kappa\int_S f(\mathbf{a}_0,\kappa)dSd\kappa = 1, \tag{5}$$

where S represents any spherical surface inside the material domain. Note that the approach proposed may also be used to model discrete distributions of fibers, by taking $f(\mathbf{a}_0,\kappa) = \sum_i^n \delta(\mathbf{a}_0^i,\kappa^i)$ where $\delta(\cdot)$ is the Dirac delta. In the case $f(\mathbf{a}_0,\kappa) = \delta(\mathbf{a}_0,\kappa)$, a model with a single family of fibers is retrieved. We restrict our attention here to fiber-reinforced hyperlastic materials whose strain energy density is a function $W(I_1, I_4)$ only of the first and fourth invariant and where the contribution of each invariants can be isolated by an additive decomposition

$$W(I_1,I_4) = W_m(I_1) + W_f(I_4) \tag{6}$$

Following [1,2,3], we assume the contribution of I_1 to be Neo-Hookean

$$W_m(I_1) = \frac{\mu}{2}(I_1 - 3) \tag{7}$$

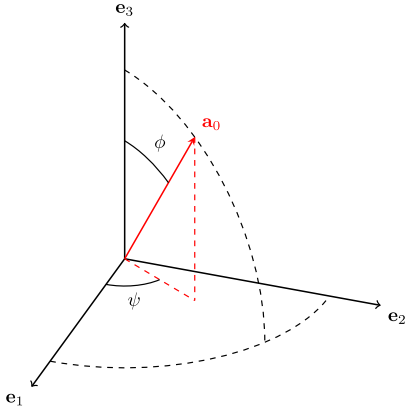

(a) Spherical coordinates employed in Equation 1. $\phi \in [0,\pi)$ is the inclination, $\psi \in [0,\pi)$ the azimuth.

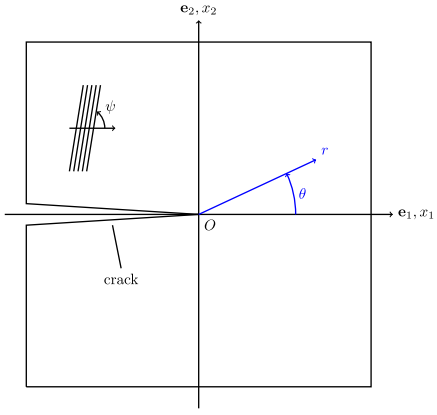

(b) A thin sheet of fiber-reinforced hyperelastic material with an edge crack. Reference configuration of the plane stress problem with both the global cartesian coordinates $x_1 - x_2$ and polar coordinates r, θ at the crack tip.

Fig. 1. Reference frames assumed in this work.

and that of I_4 to be, for any family of fibers [1]

$$w_f(I_4(\mathbf{a}_0,\kappa)) = \kappa\frac{\mu}{2}\left(I_4 + 2I_4^{-\frac{1}{2}} - 3\right) \tag{8}$$

The total contribution to the strain energy of the fourth invariant can be thus calculated as

$$W_f(I_4) = \frac{1}{4\pi}\int_\kappa\int_S f(\mathbf{a}_0,\kappa)w(I_4(\mathbf{a}_0,\kappa))dSd\kappa. \tag{9}$$

The full form of our chosen strain energy density function is thus

$$W(I_1,I_4) = \frac{\mu}{2}(I_1-3) + \frac{\mu}{4\pi}\int_0^\infty\int_0^\pi\int_0^\pi f(\mathbf{a}_0,\kappa)\kappa \left(\left(\mathbf{a}_0^T\mathbf{C}\mathbf{a}_0\right) + 2\left(\mathbf{a}_0^T\mathbf{C}\mathbf{a}_0\right)^{-\frac{1}{2}} - 3\right)\sin\phi d\phi d\psi d\kappa, \tag{10}$$

where the integration over the spherical surface S has been written explicitly in its inclination ϕ and azimuthal ψ components and the integration over κ has been specified over the range $[0,\infty)$.

We consider incompressible materials only and thus the second Piola-Kirchhoff tensor is calculated as

$$\mathbf{S} = 2\frac{\partial W}{\partial \mathbf{C}} - p\mathbf{C}^{-1}, \tag{11}$$

where the second term accounts for the incompressibily constraint and $p = -\frac{1}{3}tr\sigma$, with σ the Cauchy (true) stress tensor.

Substituting Eq. (10) into (11), we get

$$\begin{aligned}\mathbf{S} &= 2\frac{\partial W_m}{\partial I_1}\mathbf{I} + \frac{1}{2\pi}\int_\kappa\int_S f(\mathbf{a}_0,\kappa)\frac{\partial w_f}{\partial I_4}\mathbf{a}_0\otimes\mathbf{a}_0 dSd\kappa - p\mathbf{C}^{-1}\\ &= \mu\mathbf{I} + \frac{\mu}{4\pi}\int_\kappa\int_S f(\mathbf{a}_0,\kappa)\kappa\left(1 + I_4^{-\frac{3}{2}}\right)\mathbf{a}_0\otimes\mathbf{a}_0 dSd\kappa - p\mathbf{C}^{-1}.\end{aligned} \tag{12}$$

The first Piola-Kirchhoff stress tensor $\mathbf{P}$ is obtained from $\mathbf{S}$ as $\mathbf{P} = \mathbf{F}\mathbf{S}$. Taking into account Equation (12), we have

$$\mathbf{P} = \mu\mathbf{F} + \frac{\mu}{4\pi}\int_\kappa\int_S f(\mathbf{a}_0,\kappa)\kappa\left(1 + I_4^{-\frac{3}{2}}\right)\mathbf{F}\mathbf{a}_0\otimes\mathbf{a}_0 dSd\kappa - p\mathbf{F}^{-T}. \tag{13}$$

3. Plane stress

Given that many applications of highly stretchable fiber-reinforced polymers are in the form of thin sheets [39–41] and that tissues as well can be modeled as such [16,23,25], we restrict our analysis to this structural configuration and thus, following [42], to plane stress conditions. It is worth to remark here that the assumption of plane stress is key for all the derivations and results presented in this work. Extension to axisymmetric and/or generic 3D configurations is thus not straightforward and will require further work to explore it. The results shall thus be considered as applicable only to thin sheets, for which assumptions of plane stress reasonably apply. We assume that the thin sheet belongs to the plane where the unit vectors $\mathbf{e}_1,\mathbf{e}_2$ lie, and that $\mathbf{e}_3$ coincides with the thickness direction and denotes the normal to the plane of planar stress state. To enforce the state of plane stress we require that

$$\mathbf{e}_3^T\mathbf{a}_0 = 0 \tag{14}$$

for any family of fibers, which restricts the fiber orientations to $\phi = \frac{\pi}{2}$ and thus reduces Eq. (1) to

$$\mathbf{a}_0 = \cos\psi\mathbf{e}_1 + \sin\psi\mathbf{e}_2. \tag{15}$$

In agreement with the assumption of plane stress in the plane $1-2$, it holds that $P_{33} = 0$ and $P_{\alpha\beta,3} = 0$ with $\alpha,\beta = 1,2$, where the comma stands for the partial derivative. As $F_{\alpha 3} = F_{3\alpha} = 0$ with $\alpha = 1,2$, the component F_{33} is equal to the out-of-plane stretch $\lambda_3 = \lambda$, i.e. $F_{33} = \lambda$. By calling J the jacobian of the deformation gradient restricted to the plane of planar stress, i.e. $J = det(F_{\alpha\beta})$ with $\alpha,\beta = 1,2$, the satisfaction of the incompressibility constraint requires that $J = \lambda^{-1}$ and $C_{33}^{-1} = \lambda^{-2}$, which implies that $P_{\alpha 3} = P_{3\alpha} = 0$. The equilibrium equations in the absence of body forces are thus reduced to $P_{\alpha\beta,\beta} = 0\alpha,\ \beta = 1,2$. Inserting the expression $C_{33}^{-1} = \lambda^{-2}$ into the third of Eq. (12), and taking into account the condition of Eq. (14), we obtain the expression of p as a function of λ as $p = \mu\lambda^2$. Thanks to the latter equality, noting that $JF_{\beta\alpha}^{-1} = \varepsilon_{\alpha\gamma}\varepsilon_{\beta\nu}F_{\gamma\nu} = \varepsilon_{\alpha\gamma}\varepsilon_{\beta\nu}y_{\gamma,\nu}$, and recalling that $F_{\alpha\beta} = y_{\alpha,\beta}$, the plane components of the first Piola-Kirchhoff stress tensor can be written as (in indicial notation, all indices vary in the range $1,2$)

$$P_{\alpha\beta} = \mu\left(y_{\alpha,\beta} + y_{\alpha,\nu}\frac{1}{4\pi}\int_\kappa\int_S f(\mathbf{a}_0,\kappa)\kappa\left(1+\lambda_f^{-3}\right)a_\nu^0 a_\beta^0 dSd\kappa - \lambda^3\varepsilon_{\alpha\gamma}\varepsilon_{\beta\nu}y_{\gamma,\nu}\right), \tag{16}$$

where the term $y_{\alpha,\nu}$ has been factored out of the integral as it does not depend on the fiber orientation. Using Eq. (16), the traction vector t_α over a surface of normal n_β can be evaluated as $t_\alpha = P_{\alpha\beta}n_\beta$. Finally, the plane stress quilibrium equations are

$$\begin{aligned}&y_{\alpha,\beta\beta} + y_{\alpha,\nu\beta}\frac{1}{4\pi}\int_\kappa\int_S f(\mathbf{a}_0,\kappa)\kappa\left(1+\lambda_f^{-3}\right)a_\nu^0 a_\beta^0 dSd\kappa\\ &\quad + y_{\alpha,\nu}\frac{1}{4\pi}\int_\kappa\int_S f(\mathbf{a}_0,\kappa)\kappa\left(1+\lambda_f^{-3}\right)_{,\beta}a_\nu^0 a_\beta^0 dSd\kappa - \lambda^3\varepsilon_{\alpha\gamma}\varepsilon_{\beta\nu}y_{\gamma,\nu\beta}\\ &\quad = 0,\end{aligned} \tag{17}$$

which are solved under the condition of traction-free crack faces

$$\begin{aligned}&\left(y_{\alpha,\beta} + y_{\alpha,\nu}\frac{1}{4\pi}\int_\kappa\int_S f(\mathbf{a}_0,\kappa)\kappa\left(1+\lambda_f^{-3}\right)a_\nu^0 a_\beta^0 dSd\kappa - \lambda^3\varepsilon_{\alpha\gamma}\varepsilon_{\beta\nu}y_{\gamma,\nu}\right)n_\beta\\ &= 0 \text{at}\quad x_1 \le 0,\ x_2 = 0.\end{aligned} \tag{18}$$

4. Asymptotic boundary value problem and its solution

4.1. Asymptotic boundary value problem

We analyze the case of an edge crack lying on the x_1 axis, as depicted in Fig. 1b[1], and we focus on the determination of stress and deformation fields in the vicinity of the crack tip under the condition of traction-free crack faces. We will determine the crack tip fields up to a set of constants, whose value depends on the applied far-field boundary conditions.

Referring to crack tip polar coordinates $r-\theta$ as shown in Fig. 1b, we seek solutions to the equilibrium equations (17) such that the in-plane stretches are singular, i.e. $\lambda_\alpha = O(r^{m-1})$ as $r\to 0$, with $-\pi \le \theta \le \pi$, $\alpha,\beta = 1,2$ and $m \in \mathbb{R}$. Following [43,42], we also require that the out-of-plane stretch behaves asymptotically as $\lambda = J^{-1} = O(r^q)$ as $r\to 0$, with $-\pi \le \theta \le \pi$ and $q \in \mathbb{R}$, which simplifies the asymptotic form of the equilibrium equations by forcing some components of the deformation gradient to be unbounded. In particular, the fiber stretch $\lambda_f \to \infty$ and thus $\lambda \to 0$ for $r\to 0$. Thanks to the assumptions made, the asymptotic solution must satisfy

[1] Notice that in Fig. 1b the fiber orientation angle ψ is defined with respect to the axis $\mathbf{e}_1$ of undeformed coordinates x_1 in agreement with the spherical coordinates employed in Eq. (1) and defined in Fig. 1a. When working with a 2D system, it is possible to define the fiber orientation angle with respect to the axis $\mathbf{e}_2$ of undeformed coordinates x_2. This is the approach taken in [5], where such angle is referred to as ϕ. Observe that $\phi = \frac{\pi}{2} - \psi$ and thus $\cos\psi = \sin\phi$, $\sin\psi = \cos\phi$.

$$y_{\alpha,\beta\beta}+y_{\alpha,\nu\beta}\frac{1}{4\pi}\int_\kappa\int_S f(\mathbf{a}_0,\kappa)\kappa a_\nu^0 a_\beta^0 dS d\kappa=0, \tag{19}$$

subject to

$$\left(y_{\alpha,\beta}+y_{\alpha,\nu}\frac{1}{4\pi}\int_\kappa\int_S f(\mathbf{a}_0,\kappa)\kappa a_\nu^0 a_\beta^0 dS d\kappa\right)n_\beta|_{\theta=\pm\pi}=0. \tag{20}$$

4.2. Transformation to canonical form

The solution to Eq. (19) has been already discussed in detail in [5] for the cases of one and two families of perfectly aligned fibers oriented at different angles, here we will recall only the key concepts important to understand the results presented. In analogy with anisotropic linearly elastic antiplane crack problems [44], we introduce the following notation:

$$\begin{aligned} c_{44} &= 1+\frac{1}{4\pi}\int_\kappa\int_\phi f(\psi,\kappa)\kappa\sin^2\psi d\psi d\kappa \\ c_{45} &= \frac{1}{4\pi}\int_\kappa\int_\phi f(\psi,\kappa)\kappa\sin\psi\cos\psi d\psi d\kappa \\ c_{55} &= 1+\frac{1}{4\pi}\int_\kappa\int_\phi f(\psi,\kappa)\kappa\cos^2\psi d\psi d\kappa, \end{aligned} \tag{21}$$

by which the asymptotic governing equations (19) and boundary conditions (20) are reduced to the following system of equations:

$$\begin{cases} c_{55}y_{\alpha,11}+2c_{45}y_{\alpha,12}+c_{44}y_{\alpha,22}=0 \\ (c_{45}y_{\alpha,1}+c_{44}y_{\alpha,2})|_{\theta=\pm\pi}=0. \end{cases} \tag{22}$$

By introducing the linear transformation $\eta_i=A_{ij}x_j$, $\frac{\partial\eta_i}{\partial x_j}=A_{ij}$ with

$$\mathbf{A}=\begin{bmatrix} \sqrt{\frac{c_{44}}{c_{44}c_{55}-c_{45}^2}} & -\frac{c_{45}}{c_{44}}\sqrt{\frac{c_{44}}{c_{44}c_{55}-c_{45}^2}} \\ 0 & \sqrt{\frac{1}{c_{44}}} \end{bmatrix}, \tag{23}$$

Eq. (22) are transformed, in the plane $\eta_1-\eta_2$, to their canonical form:

$$\begin{cases} \frac{\partial^2 y_\alpha}{\partial\eta_1^2}+\frac{\partial^2 y_\alpha}{\partial\eta_2^2}=0 \qquad \rho=(\eta_1^2+\eta_2^2)^{\frac{1}{2}}\to 0 \\ \frac{\partial y_\alpha}{\partial\eta_2}=0 \qquad \eta_1\le 0,\ \eta_2=0 \text{ or } \varphi=\tan^{-1}\left(\frac{\eta_2}{\eta_1}\right)=\pm\pi, \end{cases} \tag{24}$$

in which we dropped the comma notation for partial derivatives to highlight the change of variables and introduced a system $\rho-\varphi$ of crack tip polar coordinates in the plane $\eta_1-\eta_2$. It is worth noting that the canonical form 24 correspond to the asymptotic plane stress governing equations for a crack in an isotropic Neo-Hookean sheet [42]. Given the solution $\tilde{y}_\alpha$ of the isotropic problem [42] in the coordinates ρ,ψ

$$\tilde{y}_\alpha=\sum_m \rho^{\frac{m}{2}}\tilde{\nu}_m(\varphi) \quad as \quad \rho\to 0 \tag{25}$$

with

$$\tilde{\nu}_m=\begin{cases} p_m\sin\left(\frac{m}{2}\varphi\right) & for \quad m=2n-1 \\ q_m cos\left(\frac{m}{2}\varphi\right) & for \quad m=2n \end{cases} \qquad with \quad n\in \text{자연수}, n>0, \tag{26}$$

The solution y_α of the anisotropic problem in the coordinates r,θ can found as

$$y_\alpha=\sum_m r^{\frac{m}{2}}\left((A_{11}\cos(\theta)+A_{12}\sin(\theta))^2+(A_{22}\sin(\theta))^2\right)^{\frac{m}{4}}\nu_m(\theta) \quad as \quad \rho\to 0 \tag{27}$$

with

$$\nu_m=\begin{cases} p_m sin\left(\frac{m}{2}tan^{-1}\left(\frac{A_{22}sin(\theta)}{A_{11}cos(\theta)+A_{12}sin(\theta)}\right)\right) & for \quad m=2n-1 \\ q_m cos\left(\frac{m}{2}tan^{-1}\left(\frac{A_{22}sin(\theta)}{A_{11}cos(\theta)+A_{12}sin(\theta)}\right)\right) & for \quad m=2n \end{cases} \qquad with \quad n\in \text{자연수}, n>0. \tag{28}$$

5. Crack tip integrals

5.1. Asymptotically path-independent interaction integral

Following [5], it is possible to evaluate all the crack tip parameters by introducing asymptotically path-independent interaction integrals of the type

$$I^{y_\alpha}(x_i)=\lim_{\Gamma\to 0}\int_\Gamma\left(P_{\alpha j}y_j^{aux}n_1-P_{\alpha j}y_{,1}^{aux}n_j-P_j^{aux}y_{\alpha,1}n_j\right)d\Gamma, \quad \alpha=1,2. \tag{29}$$

In the previous equation, y^{aux} is an auxiliary field satisfying the asymptotic boundary value equations and P_j^{aux} is the conjugated auxiliary stress evaluated as $P_j^{aux}=y_{,k}^{aux}D_{kj}$, where D_{kj} are the components of the matrix

$$\mathbf{D}=\begin{bmatrix} c_{55} & c_{45} \\ c_{45} & c_{44} \end{bmatrix} \tag{30}$$

It has been shown [5] that the latter is related to the asymptotic interaction integral $\tilde{I}^{y_\alpha}(\eta_i)$ in the scaled coordinate system $\eta_1-\eta_2$ by $I^{y_\alpha}(x_i)=\sqrt{c_{44}}\,\tilde{I}^{y_\alpha}(\eta_i)$. As in the scaled coordinate system the problem is equivalent to that of an isotropic Neo-Hookean material, it has been shown [4] that

$$\begin{cases} I^{y_\alpha}(x_i)=\sqrt{c_{44}}\ \frac{\pi}{2}\mu p_\alpha \quad for \quad \tilde{y}^{aux}=\rho^{\frac{1}{2}}\sin\frac{\varphi}{2} \\ I^{y_\alpha}(x_i)=-2\sqrt{c_{44}}\,\pi\mu q_\alpha \quad for \quad \tilde{y}^{aux}=\ln\rho \end{cases} \tag{31}$$

where p_α,q_α, $with\ \alpha=1,2$ are parameters whose values depend on far-field boundary conditions.

5.2. Numerical realization of crack tip integrals

We realize the crack tip integrals introduced in Section 5.1 in the FEM model (later presented in Section 6.1) in the form of domain integrals [5]. Given a test function g representing an arbitrary virtual displacement of the crack tip, the crack tip integrals have the following domain-integral form:

$$I^{y_\alpha}=\int_A\left(-P_{\alpha j}y_j^{aux}\frac{\partial g}{\partial x_1}+\left(P_{\alpha j}y_{,1}^{aux}n_j+P_j^{aux}y_{\alpha,1}n_j\right)\frac{\partial g}{\partial x_1}\right)dA. \tag{32}$$

It is possible to show [5] that the integrand of the term $\int_A(\cdot)_{,j}gdA$ is asymptotically divergence-free, i.e. if the contours are taken in the region of dominance of the asymptotic crack tip fields. The function g is assumed to be $\frac{r_0-r}{r_0}$, where r_0 is the radius of the circular path of the corresponding contour integral, such that $g=0$ on the domain boundary and $g=1$ at the crack tip. Further details can be found in [5].

5.3. Coordinate-based method

Similar to [5], a coordinate-based approach in the form of a P_k contour integral [45] is used to validate the results of the interaction integrals. Accordingly, the coefficients of the asymptotic expansion are evaluated as

$$p_1 = \frac{y_1^n(r_0,\pi) - y_1^n(r_0,-\pi)}{(4A_{11}r_0)^{\frac{1}{2}}} \qquad p_2 = \frac{y_2^n(r_0,\pi) - y_2^n(r_0,-\pi)}{(4A_{11}r_0)^{\frac{1}{2}}} \qquad q_1 = \frac{y_1^n(r_0,0)}{A_{11}r_0}, \tag{33}$$

where $y_i^n(r_0,\theta), i = 1,2$ are the deformed coordinates at the point (r_0,θ) of the Finite Element mesh.

6. Numerical analysis and results

6.1. FEM model

The crack tip fields are evaluated for an edge crack in an initially rectangular strip. The strip has dimensions $L_0 \times H_0$ with $L_0 = 4H_0$ and the initial length of the crack is $0.25L_0$. The strip is subject to far-field Mode I boundary conditions of the type $y_1 = x_1|_{x_2=\pm\frac{H_0}{2}}$, $y_2 = \lambda_S x_2|_{x_2=\pm\frac{H_0}{2}}$, where λ_S is the far-field stretch in the x_2 direction. The stiffness of the matrix μ is equal to 1 MPa while the fiber-to-matrix stiffness ratio is a parameter of the analysis. The governing Eq. (18) are solved using the Finite Element Method (FEM) with an in-house code. Implementation details can be found in [5]. The domain is discretized using 8-node quadrilateral elements with 4 four Gauss integration points and the smallest element at the crack tip has a side length of about $10^{-5}H_0$.

6.2. Continuous distributions of fiber

Incorporation of data on fiber orientation in structural models of tissues requires the formulation of a probability model [46–51], i.e. the identification of the statistical distribution $f(\mathbf{a}_0,\kappa)$ that best represents the experimental measurements. In the absence of any prior knowledge, a maximum-entropy distribution should be chosen [52], such as the *Gaussian* distribution for data defined on linear domains or the *π-periodic von Mises* distribution for data defined on circular (periodic) domains [53]. While both distributions are 2-parameter bell-shaped distributions, the π-periodicity of the *von Mises* distribution takes into account the natural symmetry of a physical distribution of long continuous fibers and it is thus the best choice to incorporate data on fiber orientation into our material model. Sacks and co-workers obtained a good fit of data of fiber distribution in bovine pericardium and porcine aortic valve obtained using small angle light scattering (SALS) through application of the *Gaussian* distribution [49,50] and used it further in modeling the mechanical response of these tissues [50,54]. The *von Mises* distribution was shown in [48] to be a good fit for data gathered in [46,47] on fibril orientation in adult rabbit medial collateral ligament, and in [51] to accurately model the distribution of collagen fibers in abdominal aortic aneurysms, measured with polarized light microscopy in combination with the universal stage. Although both distributions have found application in the experimental literature, we will focus our attention on the *π-periodic von Mises* distribution, as it represents the best probability model for data defined on circular domains such as fiber orientations.

6.2.1. Von Mises distribution

We analyze a Neo-Hookean matrix reinforced by fibers with orientations distributed according to the standard π-periodic *von Mises* distribution $f_{vM}(\psi)$

$$f_{vM}(\psi) = \frac{e^{b\cos(2(\psi-\psi_0))}}{2\pi I_0(b)}, \tag{34}$$

where

$$I_0(b) = \frac{1}{\pi}\int_0^\pi e^{b\cos\psi}d\psi \tag{35}$$

is the modified Bessel function of the first kind of order zero with parameter b. Taking into account the normalization condition and considering a constant κ, the distribution $f(\psi)$ of fiber orientations is described by

$$f(\psi) = \frac{f_{vM}(\psi)}{\int_0^\pi f_{vM}(\psi)d\psi} = \frac{e^{b\cos(2(\psi-\psi_0))}}{\int_0^\pi e^{b\cos(2(\psi-\psi_0))}d\psi}. \tag{36}$$

In Eq. (36), the parameter ψ_0 represents the main direction of the fiber family while b controls the dispersion around the main direction ψ_0. Lower values of b correspond to more dispersed fibers, while higher values b corresponds to fibers whose orientations are concentrated around the main direction ψ_0. The corresponding effect on the shape of the distribution funtion $f(\psi)$ in shown in Fig. 2.

The evaluation of the contribution of the fourth invariant to the strain energy density (Eq. (9)) requires, for constant κ, an integration of the individual fiber contribution weighted by the orientation distribution $f(\psi)$ over all possible orientations. In the case of plane stress, taking into account condition (14), Eq. (9) takes the form

$$W(I_4(\psi)) = \frac{1}{2\pi}\int_0^\pi f(\psi)w(I_4(\psi))d\psi, \tag{37}$$

which can be evaluated numerically using a 12-point Gauss quadrature rule according to

$$W(I_4(\psi)) = \frac{1}{4}\sum_{n=1}^{12}\omega_n f\left(\frac{\pi}{2}(1+\xi_n)\right)w\left(I_4\left(\frac{\pi}{2}(1+\xi_n)\right)\right), \tag{38}$$

where ω_n and ξ_n are respectively the Gauss points and weights on the unit interval. The coefficients of Eq. (21) become in plane stress

$$\begin{aligned} c_{44} &= 1 + \frac{\kappa}{2\pi}\int_0^\pi f(\psi)\sin^2\psi d\psi \\ c_{45} &= \frac{\kappa}{2\pi}\int_0^\pi f(\psi)\sin\psi\cos\psi d\psi \\ c_{55} &= 1 + \frac{\kappa}{2\pi}\int_0^\pi f(\psi)\cos^2\psi d\psi, \end{aligned} \tag{39}$$

which are as well evaluated using a 12-point Gauss quadrature rule. In Fig. 3, it is shown the effect of the distribution parameters b and ψ_0 on the coefficients c_{44}, c_{45}, c_{55} of transformation 21.

For a given value of b, it is possible to observe that c_{55} decreases for increasing values of ψ_0, reaching its maximum at $\psi_0 = 0$ and its minimum at $\frac{\pi}{2}$. c_{44} shows the opposite behavior, increasing for increasing values of ψ_0, with the maximum at $\psi_0 = \frac{\pi}{2}$ and its minimum at 0. On the other hand, the coefficient c_{45} reaches its peak value at $\frac{\pi}{4}$ and is equal to zero both at 0 and $\frac{\pi}{2}$. Finally, observe that for $b > 5$ the dependency on the value of b is practically non-existent, which implies that the behavior of the *von Mises* distribution is for practical purposes undistinguishable from the case of perfectly aligned fibers as $c_{ij}(b > 5) \sim c_{ij}(b\to\infty)$, where $b\to\infty$ corresponds to the case of perfectly aligned fibers (see Fig. 3a). To investigate the effect of fiber dispersion, b should be chosen < 5, with most of the variability concentrated in the range $(0,3)$. As we are on the other hand interested in investigating the effect of the main fiber orientation on the crack tip fields, we will set b to a value higher than 5.

We select in particular $b = 10$ and analyze 3 different cases in which the main fiber orientation ψ_0 is respectively equal to $0, \frac{\pi}{4}, \frac{\pi}{2}$, with an applied stretch $\lambda_S = 2$ and fiber-to-matrix stiffness ratio $\kappa = 2$. As explained in [5], to have an open crack in the case of large deformation, the leading order term $p_2\rho^{\frac{1}{2}}$ of the asymptotic expansion of y_2 must be the dominant one, i.e. it must hold that $p_2\rho^{\frac{1}{2}} >> q_2\rho$, where $q_2\rho$ is the second order term of the expansion. Our numerical analysis confirms that q_2 is approximately 0 in all examples considered and it is thus not reported. We thus evaluate the coefficients p_1, q_1, p_2 of the leading terms of the asymptotic expansion using interaction integrals (denoted by Ξ^I) and the coordinate-based method (denoted by Ξ^C). Results are reported in

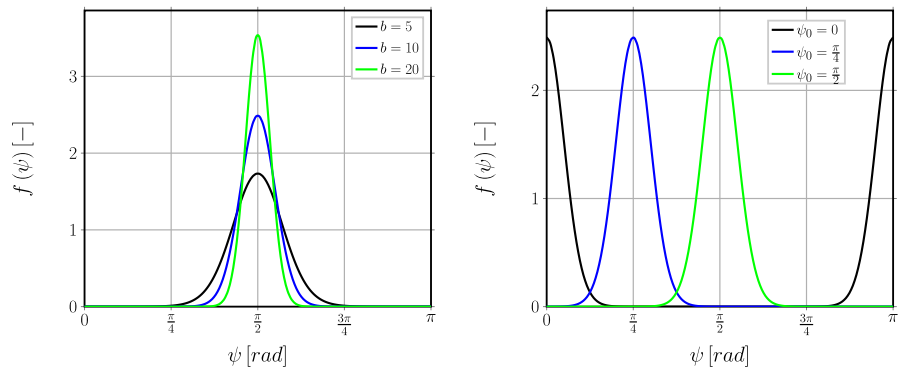

(a) $\psi_0 = \frac{\pi}{2}$ (b) $b = 10$

Fig. 2. Effect of the parameters b and ψ_0 on the shape of the distribution function $f(\psi)$.

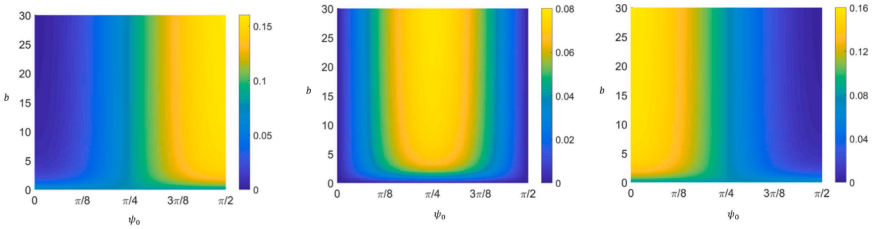

(a) $\frac{c_{44}-1}{\kappa}$ (b) $\frac{c_{45}}{\kappa}$ (c) $\frac{c_{55}-1}{\kappa}$

Fig. 3. Effect of the parameters b and ψ_0 on the coefficients c_{44}, c_{45}, c_{55} of transformation 21.

Table 1. The agreement between the methods is good (to the second and often to third decimal value) and thus in the following we will use only the values computed with the interaction integrals to evaluate the analytical solution previously determined.

In Fig. 4, it is possible to observe the good agreement between FEM results and analytical predictions for both the circumferential variation (at $\frac{r}{H_0} = 10^{-4}$) and radial variation (at $\theta = \pi$) of the deformed coordinates y_1 and y_2. For $\psi_0 = 0, \frac{\pi}{2}$, notice that $p_1 = 0$ (see Table 1) and $c_{45} = 0$ (see Fig. 3), which imply that in Eq. (23) $A_{11} = \frac{1}{\sqrt{c_{55}}}, A_{12} = 0$, $A_{22} = \frac{1}{\sqrt{c_{44}}}$ and thus that from Eqs. (25) and (26) we have $y_1 \sim q_1 \rho \cos\psi = q_1 \eta_1 = \frac{q_1}{\sqrt{c_{55}}} r\cos\theta$. This is evident, for $\psi_0 = 0, \frac{\pi}{2}$, from the symmetry of $y_1(\theta)$ in Fig. 4a and the $y_1 \sim r$ behavior in Fig. 4c.

The previous observations imply that, under far-field Mode I boundary conditions $y_1 = x_1|_{x_2=\frac{H_0}{2}}, y_2 = \lambda_S x_2|_{x_2=\frac{H_0}{2}}$, the crack tip experiences for $\psi_0 = 0, \frac{\pi}{2}$ a pure Mode I deformation similarly to what occurs for an isotropic Neo-Hookean material. However, notice that the behavior is not isotropic in the region of dominance of the asymptotic solution as $c_{44} \neq c_{55}$ and thus Eq. (22) becomes $c_{55} y_{\alpha,11} + c_{44} y_{\alpha,22} = 0$. Recalling the matrix D introduced in Eq. (30), in the region of asymptotic dominance the first Piola-Kirchhoff and the Cauchy stress tensors are $\mathbf{P} = \mu \mathbf{FD}$ and $\sigma = \mu \mathbf{FDF}^T$. For $\psi_0 = 0, \frac{\pi}{2}$, with $c_{45} = 0, c_{44} \neq c_{55}$, they can be expressed respectively as $\mathbf{P} = \mu \left[c_{55}\mathbf{y}_{,1} | c_{44}\mathbf{y}_{,2} \right]$ and $\sigma = \mu \left(c_{55}\mathbf{y}_{,1}\mathbf{y}_{,1}^T + c_{44}\mathbf{y}_{,2}\mathbf{y}_{,2}^T \right)$, where $\mathbf{y} = [y_1 \ y_2]^T$ is the position vector of the generic point in the deformed configuration. Thus, for an isotropic deformation field of the type $y_i = \gamma x_i$ the resultant stress field is anisotropic and for $\psi_0 = 0, \frac{\pi}{2}$ the material in the region of asymptotic dominance behaves anisotropically. This result is confirmed by the deformed configurations of the crack tips as shown in Fig. 5. The deformed configuration is symmetric with respect to the crack line $\theta = 0$ for $\psi_0 = 0, \frac{\pi}{2}$ (pure Mode I at the crack tip for far-field Mode I boundary conditions, as $c_{45} = 0$), but the shape is different (anisotropic response). In comparison, for $\psi_0 = \frac{\pi}{8}, \frac{\pi}{4}, \frac{3\pi}{8}$, the deformed configuration is neither symmetric (Mixed Mode at the crack tip for far-field Mode I boundary conditions, as $c_{45} \neq 0$) nor similar to each other (anisotropic response).

Fig. 4b shows that at the crack faces ($\theta = \pm\pi$) the value of y_2 is the lowest for $\psi_0 = 0$ and the highest for $\psi_0 = \frac{\pi}{2}$. A *von Mises* distribution of fibers centered on $\psi_0 = \frac{\pi}{2}$, i.e. normal to the direction of crack propagation, promotes the maximum opening of the crack, as fiber stretch occurs on average normal to crack faces (recall the decomposition of the deformation gradient adopted in the current model following [1–3]) and thus acts to open the crack. On the other hand, for a distribution centered on $\psi_0 = 0$, i.e. parallel to the direction of crack propagation, fiber stretch occurs on average parallel to crack faces and thus does not

Table 1
Asymptotic expansion coefficients p_1, q_1, p_2 in the *von Mises* distribution case evaluted using interaction energy integrals, denoted by Ξ^I, and the coordinate based method, denoted by Ξ^C. Main fiber orientation $\psi_0 = 0, \frac{\pi}{4}, \frac{\pi}{2}$, fiber dispersion $b = 5$, applied stretch $\lambda_S = 2$, ratio of fiber to matrix stiffness $\kappa = 10$.

	$\psi_0 = 0$			$\psi_0 = \frac{\pi}{4}$			$\psi_0 = \frac{\pi}{2}$		
	p_1	p_2	q_1	p_1	p_2	q_1	p_1	p_2	q_1
Ξ^I	0.000	1.204	0.589	0.061	1.567	0.644	0.000	1.393	0.727
Ξ^C	0.000	1.203	0.585	0.061	1.599	0.640	0.000	1.377	0.723

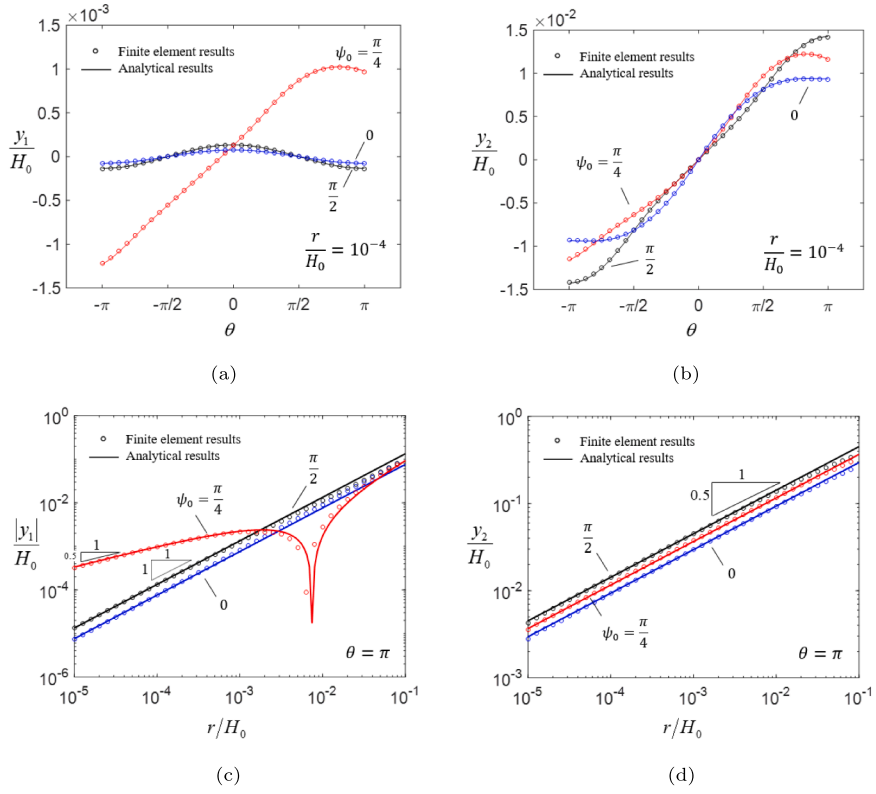

Fig. 4. Circumferential (11, 12) and radial (13, 14) variation of normalized deformed coordinates $\frac{y_1}{H_0}$ (11, 13) and $\frac{y_2}{H_0}$ (12, 14) for main fiber orientation $\psi_0 = 0, \frac{\pi}{4}, \frac{\pi}{2}$, fiber dispersion $b = 5$, applied stretch $\lambda_S = 2$, ratio of fiber to matrix stiffness $\kappa = 10$. Open circles correspond to FEM results, solid line to the analytical prediction based on the results of Eq. (27).

affect their deformation, which is in this case driven by the matrix-dominated shear (the second component of the deformation gradient decomposition of [1–3]).

It was shown in [5] that, in the case of a single family of fibers oriented at $\psi = 0$, there exists a cusp in the variation of y_1 with respect to θ for fiber-to-matrix stiffness ratio $\kappa > 1$. No such cusp can be observed for y_1 in Fig. 4a in the case of a fiber distribution centered on $\psi_0 = 0$. This means, interestingly, that the effect of eigenmodes higher than the second is negligible in the case of a distribution of fibers.

For $\psi_0 = \frac{\pi}{4}$, the slope of y_1 in Fig. 4c is equal to $\frac{1}{2}$, differently from the cases $\psi_0 = 0, \frac{\pi}{2}$. This is due to the fact that $p_1 \neq 0$ (see Table 1) and thus the first order eigenmode plays an important role in the behavior of y_1. In particular, $y_1 \sim p_1 \rho^{\frac{1}{2}} - q_1 \rho \sim p_1 \sqrt{A_{11}} r^{\frac{1}{2}} - q_1 A_{11} r$ which implies that $y_1 \sim 0$ at $r \sim \frac{p_1^2}{q_1^2 A_{11}}$, corresponding to the drop in Fig. 4c.

In Fig. 6, the components P_{21} and P_{22} of the first Piola-Kirchhoff stress and σ_{22} of the Cauchy stress tensor are reported. It can be observed that the agreement between FEM results and analytical predictions is good. P_{21} (Fig. 6a) has its extrema in correspondence of the crack faces at $\theta = \pm\pi$, P_{22} (Fig. 6b) reaches its maximum value always in the range $-\frac{\pi}{2} < \theta < \frac{\pi}{2}$ and is equal to 0 for $\theta = \pm\pi$, verifying the condition of traction-free crack faces. Notice that for $\psi_0 = 0, \frac{\pi}{2}$, P_{21} is an odd function of θ while P_{22} is an even function of θ. Given that $c_{45} = 0$ (see Fig. 3c) for both $\psi_0 = 0, \frac{\pi}{2}$, we have

$$P_{21} = -\frac{1}{2}\mu p_2 \sqrt{c_{55}} \rho^{-\frac{1}{2}} \sin\left(\frac{\varphi}{2}\right) \qquad P_{22} = \frac{1}{2}\mu p_2 \sqrt{c_{44}} \rho^{-\frac{1}{2}} \cos\left(\frac{\varphi}{2}\right) \tag{40}$$

with

$$\rho = \frac{1}{\sqrt{c_{55}}} r \cos\theta \sqrt{1 + \frac{c_{55}}{c_{44}} \tan^2\theta} \qquad \varphi = \tan^{-1}\left(\sqrt{\frac{c_{55}}{c_{44}}} \tan\theta\right), \tag{41}$$

which means that φ is a monotonic function of θ, ρ is an even function of θ (as $\cos\theta, \tan^2\theta, \sqrt{1 + \frac{c_{55}}{c_{44}} \tan^2\theta}$ are all even), and thus P_{21} is an odd function of θ (product of even function $\rho^{-\frac{1}{2}}$ with odd function $\sin\left(\frac{\varphi}{2}\right)$) and P_{22} is an even function of θ (product of even function $\rho^{-\frac{1}{2}}$ with even function $\sin\left(\frac{\varphi}{2}\right)$). Notice that, on the other hand, for $\psi_0 = \frac{\pi}{4}$ no symmetry is present.

It was observed in [5] that the extrema θ_e of σ_{22} satisfy the relationship $\theta_e + \psi_0 = 0, \pm\frac{\pi}{2}, \pm\pi, \cdots$. Interestingly, it remains valid also in the case of a *von Mises* distribution of fiber orientations (see Fig. 6c) with ψ_0 the main direction of alignment of the fibers. Finally, Fig. 6d confirms, at $\theta = 0$, the expectation that $\sigma_{22} \sim r^{-1}$ for $r \to 0$ and that $\frac{\sigma_{22}}{\mu} = \lambda_S^2 - \frac{\lambda_S^2 \kappa}{2\pi} \int f(\psi) \left(1 - \lambda_f^{-3}\right) \lambda^f \cos^2\psi d\psi$ for $r \to \infty$.

6.3. Asymptotic isotropy at the crack tip

Recalling transformation 21, if the conditions $c_{45} = 0, c_{55} = c_{44}$ are satisfied, the governing equations are reduced to those of the isotropic problem *without* resorting to the canonical transformation. Furthermore $\mathbf{P} = c_{44}\mu\mathbf{F}$, which implies that, in the vicinity of the crack tip, the material behaves isotropically with a stiffness that is a multiple $c_{44}\mu$ of the matrix stiffness. We thus refer to this regime as *asymptotic isotropy* and we look for fiber distributions such that the conditions for its existence are satisfied.

6.3.1. Discrete case

Consider a discrete distribution of n fibers placed at regular intervals δ such that $\delta \in [0, \pi)$ with constant κ and the first of such fibers placed at a generic angle ψ (referring to the geometry of Fig. 1b). For this configuration, the conditions of asymptotic isotropy can be written as

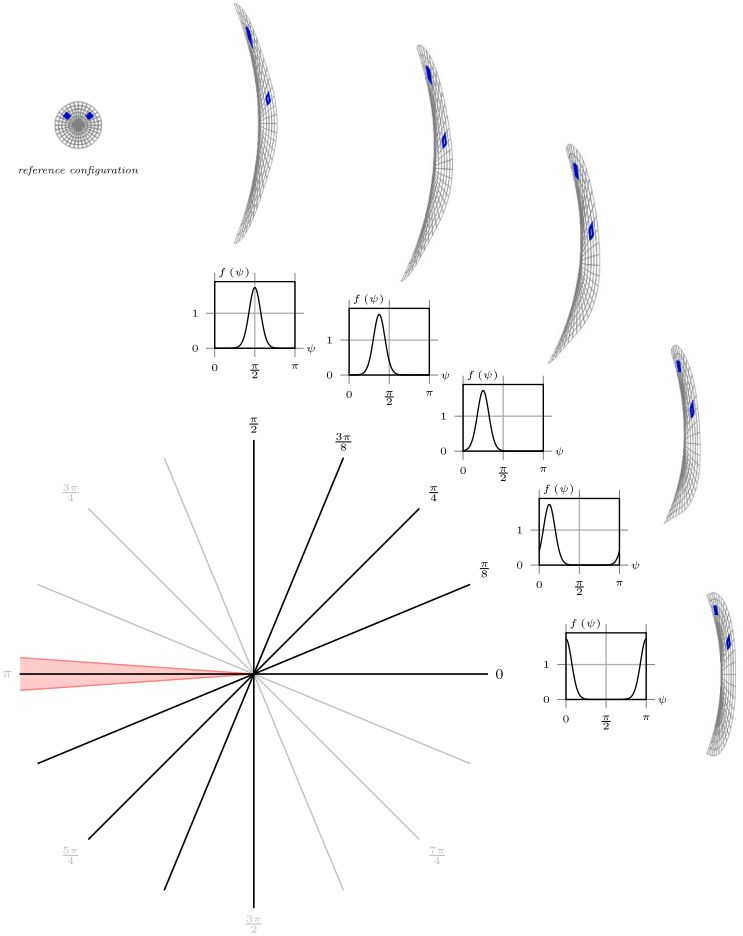

Fig. 5. Crack tip deformation for main fiber orientation (black solid line in the polar plot) $\psi_0 = 0, \frac{\pi}{8}, \frac{\pi}{4}, \frac{3\pi}{8}, \frac{\pi}{2}$, fiber dispersion $b = 5$, applied stretch $\lambda_S = 1.152$, ratio of fiber to matrix stiffness $\kappa = 10$. The position of the crack is highlighted in red in the polar plot. (For interpretation of the references to colour in this figure legend, the reader is referred to the web version of this article.)

$$\begin{cases} \sum_{i=1}^{n} sin(\psi + (i-1)\delta) cos(\psi + (i-1)\delta) = 0 \\ \sum_{i=1}^{n} sin^2(\psi + (i-1)\delta) = \sum_{i=1}^{n} cos^2(\psi + (i-1)\delta) \\ \sum_{i=1}^{n} \delta = \pi. \end{cases} \tag{42}$$

Given that $\delta = \frac{\pi}{n}$, after some trigonometric manipulations, we have in matrix–vector form

$$\sum_{i=1}^{n} \begin{bmatrix} \cos(2\psi) & -\sin(2\psi) \\ \sin(2\psi) & \cos(2\psi) \end{bmatrix} \begin{bmatrix} \cos\left(2(i-1)\frac{\pi}{n}\right) \\ \sin\left(2(i-1)\frac{\pi}{n}\right) \end{bmatrix} = 0 \qquad \forall \psi. \tag{43}$$

Given that Eq. (43) must hold for any value of ψ, the problem is reduced to finding the values of n such that

$$\sum_{i=1}^{n} \cos\left(2(i-1)\frac{\pi}{n}\right) = 0 \qquad \sum_{i=1}^{n} \sin\left(2(i-1)\frac{\pi}{n}\right) = 0, \tag{44}$$

where we recognize the arithmetic progressions of sines and cosines which are identically equal to zero [55,56]. Thus, conditions of *asymptotic isotropy* are satisfied by a discrete distribution of n fibers oriented at regular intervals of $\frac{\pi}{n}$ for any choice of $n > 1$, with $c_{44} = c_{55} = 1 + \kappa\frac{n}{2}$.

6.3.2. Continuous case

Consider a uniform distribution of fiber orientations $f_{uni}(\psi) = 1$ with $\psi \in [0, \pi)$, substituting into Eq. (39) we obtain $c_{44} = c_{55} = 1 + \frac{\kappa}{4}$ and $c_{45} = 0$, thus satisfying the conditions of *asymptotic isotropy*.

6.3.3. Numerical results

The coefficients p_1, q_1, p_2 of the leading terms of the asymptotic expansion are evaluated using interaction integrals (denoted by Ξ^I) and the coordinate-based method (denoted by Ξ^C) for 6 different cases: ① isotropic Neo-Hookean sheet (for comparison); ② 2 families of fibers, $\psi_0 = 0, \frac{\pi}{2}$, $\kappa = 1$; ③ 2 families of fibers, $\psi_0 = -\frac{\pi}{4}, \frac{\pi}{4}$, $\kappa = 1$; ④ 3 families of fibers, $\psi_0 = -\frac{\pi}{3}, 0, \frac{\pi}{3}$, $\kappa = 1$; ⑤ 4 families of fibers, $\psi_0 = 0, \frac{\pi}{2}$ with $\kappa = 1$ and $\psi_0 = -\frac{\pi}{4}, \frac{\pi}{6}$ with $\kappa = 2$; ⑥ uniform distribution of fibers. Results are reported in Table 2. In agreement with the theoretical prediction, p_1 is equal to 0 for all 6 cases, as a material behaving isotropically for $r \to 0$ would result in a pure Mode I deformation at the crack tip under pure Mode I far-field boundary conditions. In the case of *asymptotic isotropy*, it is expected that $\sigma_{22} \sim \frac{1}{4} p_2^2 \sqrt{c_{44}} r^{-1}$, which is confirmed by the numerical results reported in Fig. 7.

It is worth pointing out here that the physical origin of the *asymptotic isotropy* lies in the choice of matrix and fiber material models and thus in the form of the strain energy density as discussed in Section 2. A different (non-linear) choice of strain energy density would not have lead to the identification of fiber orientation combinations that correspond to *asymptotic isotropy*.

Finally, notice that the condition of *asymptotic isotropy* is valid in the region of dominance of the asymptotic crack tip fields while far from the crack tip the material behaves anisotropically. To show this, we consider a thin sheet with a circular hole in plane stress subject to a uniform radial stretch $\lambda_R = 0.5$. For an isotropic material, the circular hole in the

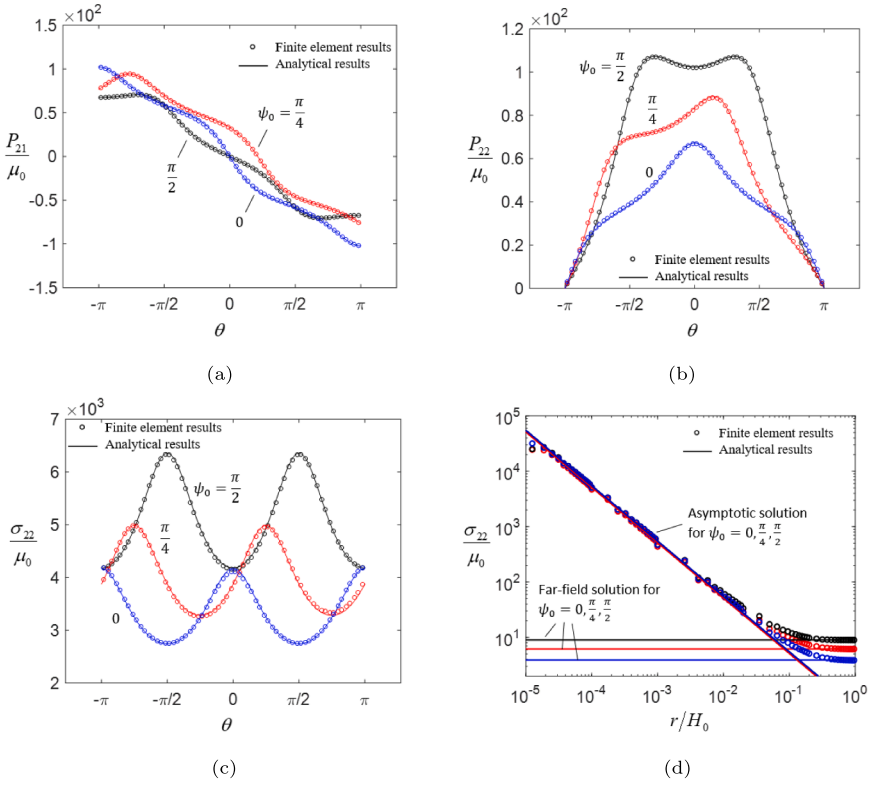

Fig. 6. Circumferential (17, 18 and 19) variation respectively of P_{21}, P_{22}, σ_{22} and radial (20) variation of σ_{22} for main fiber orientation $\psi_0 = 0, \frac{\pi}{4}, \frac{\pi}{2}$, fiber dispersion $b = 5$, applied stretch $\lambda_S = 2$, ratio of fiber to matrix stiffness $\kappa = 10$. Open circles correspond to FEM results, solid line to the analytical prediction based on the results of Eq. (27).

Table 2
Asymptotic expansion coefficients p_1, q_1, p_2 for different cases of *asymptotic isotropy* using interaction energy integrals, denoted by Ξ^I, and the coordinate based method, denoted by Ξ^C. Applied stretch $\lambda_S = 2$.

	① Isotropic (no fiber)			② 2 families of fibers $\psi_0 = 0, \frac{\pi}{2}$ $\kappa = 1\ \forall\psi_0$			③ 2 families of fibers $\psi_0 = -\frac{\pi}{4}, \frac{\pi}{4}$ $\kappa = 1\ \forall\psi_0$		
	p_1	p_2	q_1	p_1	p_2	q_1	p_1	p_2	q_1
Ξ^I	0.000	1.086	0.595	0.000	0.955	0.681	0.000	1.836	0.649
Ξ^C	0.000	1.091	0.598	0.000	0.988	0.692	0.000	1.824	0.652
	④ 3 families of fibers $\psi_0 = -\frac{\pi}{3}, 0, \frac{\pi}{3}$ $\kappa = 1\ \forall\psi_0$			⑤ 4 families of fibers $\psi_0 = 0, \frac{\pi}{2}, \kappa = 1$ $\psi_0 = -\frac{\pi}{4}, \frac{\pi}{4}, \kappa = 2$			⑥ Uniform distribution		
	p_1	p_2	q_1	p_1	p_2	q_1	p_1	p_2	q_1
Ξ^I	0.000	1.692	0.689	0.000	2.281	0.759	0.000	2.108	0.746
Ξ^C	0.000	1.673	0.693	0.000	2.275	0.763	0.000	2.106	0.750

deformed configuration is enlarged and remains circular (black solid line in Fig. 8). For an anisotropic material, the shape of the initially circular hole will changes (red solid line in Fig. 8, for the case of 2 families of fibers at $23^\circ, 39^\circ$). The deviation from circularity can thus be used as a proxy of the degree of anisotropy of the material. Observation of Fig. 8 shows that a matrix reinforced with 2 families of fibers at $0^\circ, 90^\circ$ or at $\pm 45^\circ$ is indeed anisotropic, and thus that the isotropic behavior shown in Fig. 7 occurs only in the region of dominance of the asymptotic fields.

6.4. Asymptotic universal one-to-one mapping

It is possible to interpret the transformation to canonical form introduced in Section 4.2 in a mechanical sense. Introducing the scaled deformation $\widetilde{y}_2$

$$\widetilde{y}_2 = \frac{y_2}{p_2\left(\left(A_{11}\cos\theta + A_{12}\sin\theta\right)^2 + \left(A_{22}\sin\theta\right)^2\right)^{\frac{1}{4}}\sin\left(\frac{1}{2}\tan^{-1}\left(\frac{A_{22}\sin\theta}{A_{11}\cos\theta + A_{12}\sin\theta}\right)\right)} \tag{45}$$

and scaled Cauchy stress component $\widetilde{\sigma}_{22}$

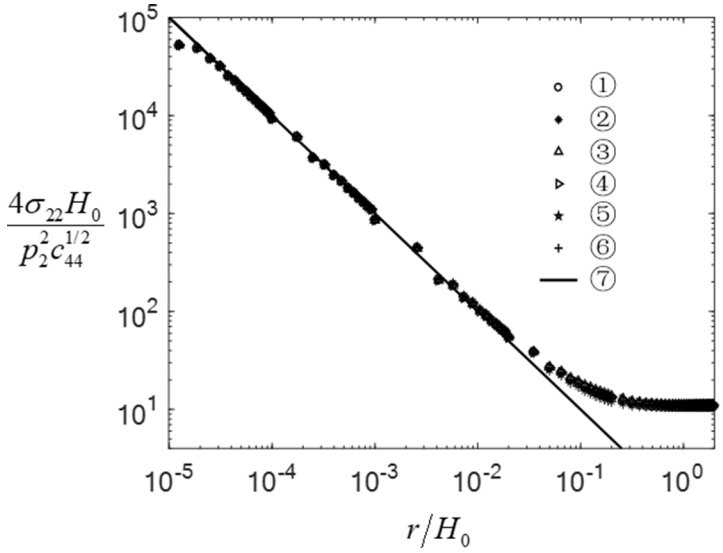

Fig. 7. Asymptotic radial behavior of normalized $\frac{4\sigma_{22}H_0}{p_2^2 c_{44}^{\frac{1}{2}}}$. Angular position $\theta = \pi$, applied stretch $\lambda_S = 2$. ① isotropic Neo-Hookean sheet (for comparison); ② 2 families of fibers, $\psi_0 = 0, \frac{\pi}{2}$, $\kappa = 1$; ③ 2 families of fibers, $\psi_0 = -\frac{\pi}{4}, \frac{\pi}{4}$, $\kappa = 1$; ④ 3 families of fibers, $\psi_0 = -\frac{\pi}{3}, 0, \frac{\pi}{3}$, $\kappa = 1$; ⑤ 4 families of fibers, $\psi_0 = 0, \frac{\pi}{2}$ with $\kappa = 1$ and $\psi_0 = -\frac{\pi}{4}, \frac{\pi}{6}$ with $\kappa = 2$; ⑥ uniform distribution of fibers; ⑦ r^{-1}

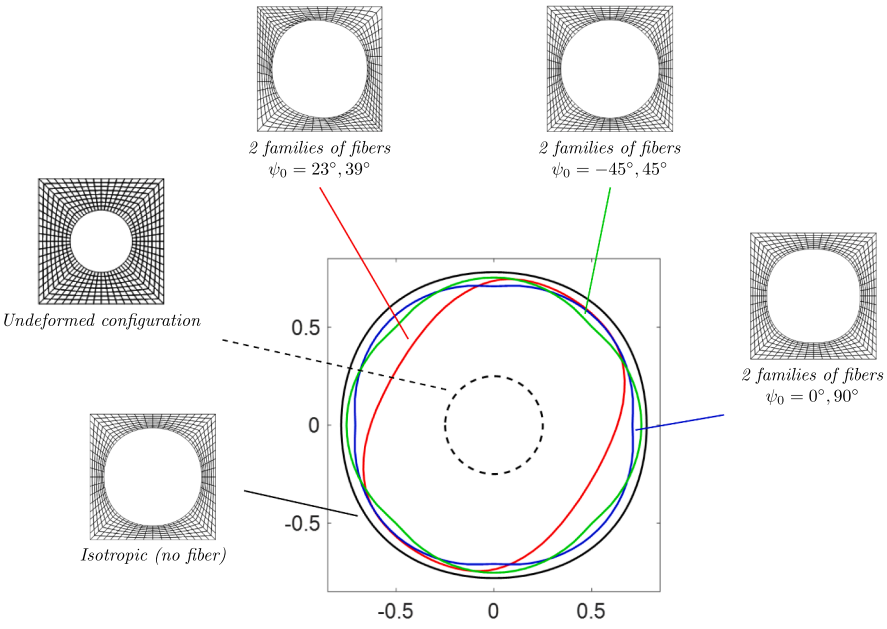

Fig. 8. Behavior of the unnotched material. Radial stretch $\lambda_R = 0.5$ applied to the outer boundary. In the main graph, the deformed configuration of the inner ring is compared between the different cases and with the undeformed configuration. *Black, dashed*: undeformed configuration; *black, solid*: isotropic Neo-Hookean sheet; *blue, solid*: 2 families of fibers, $\psi_0 = 0^\circ, 90^\circ$; *green, solid*: 2 families of fibers, $\psi_0 = -45^\circ, 45^\circ$; *red, solid*: 2 families of fibers, $\psi_0 = 23^\circ, 39^\circ$. $\kappa = 10$. (For interpretation of the references to colour in this figure legend, the reader is referred to the web version of this article.)

$$\widetilde{\sigma}_{22} = \frac{\sigma_{22}}{\frac{1}{4}\mu p_2^2 \left(\left(A_{11}\cos\theta + A_{12}\sin\theta \right)^2 + \left(A_{22}\sin\theta \right)^2 \right)^{-\frac{1}{2}}}, \tag{46}$$

it is shown in Fig. 9 that the scaled variables present an asymptotic behavior identical to that of the isotropic sheet in plane stress, i.e. $\widetilde{y}_2 \sim r^{\frac{1}{2}}$ and $\widetilde{\sigma}_{22} \sim r^{-1}$ for every value of θ and any distribution of fiber orientation and elastic properties.

von Mises distribution, $\psi_0 = \frac{\pi}{4}, b = 5, \kappa = 10$ 2 families of fibers, $\psi_0 = 23^\circ, 39^\circ$, $\kappa = 1$; isotropic Neo-Hookean sheet; 2 families of fibers, $\psi_0 = 0, \frac{\pi}{2}$, $\kappa = 1$; uniform distribution of fibers, $\kappa = 1$.

Thus, the canonical transformation of Section 4.2 provides an *asymptotic universal one-to-one mapping* that maps the asymptotic mechanical response of an anisotropic Neo-Hookean fiber-reinforced composite to that of an isotropic Neo-Hookean thin sheet. The mapping depends on the geometry and boundary conditions of the specific anisotropic problem and thus pairs one anisotropic with one isotropic configuration (*one-to-one*). As such, this mapping does not provide any significant advantage in computational cost, but it provides an interesting mechanical insight. Inspecting the structure of the linear transformation of Eq. (23), it is possible to argue that asymptotically the mechanical effect of the reinforcement in the anisotropic material is equivalent to a bi-axial stretch and in-plane shear applied to the isotropic Neo-Hookean thin sheet, i.e. to a geometric deformation of the isotropic material.

7. Conclusions

In this paper, we consider the large deformations at the crack tip of Neo-Hookean fiber reinforced composite sheet, where the orientation and elastic properties of the reinforcement are described by discrete and continuous spatial distributions. We adopt the material behavior

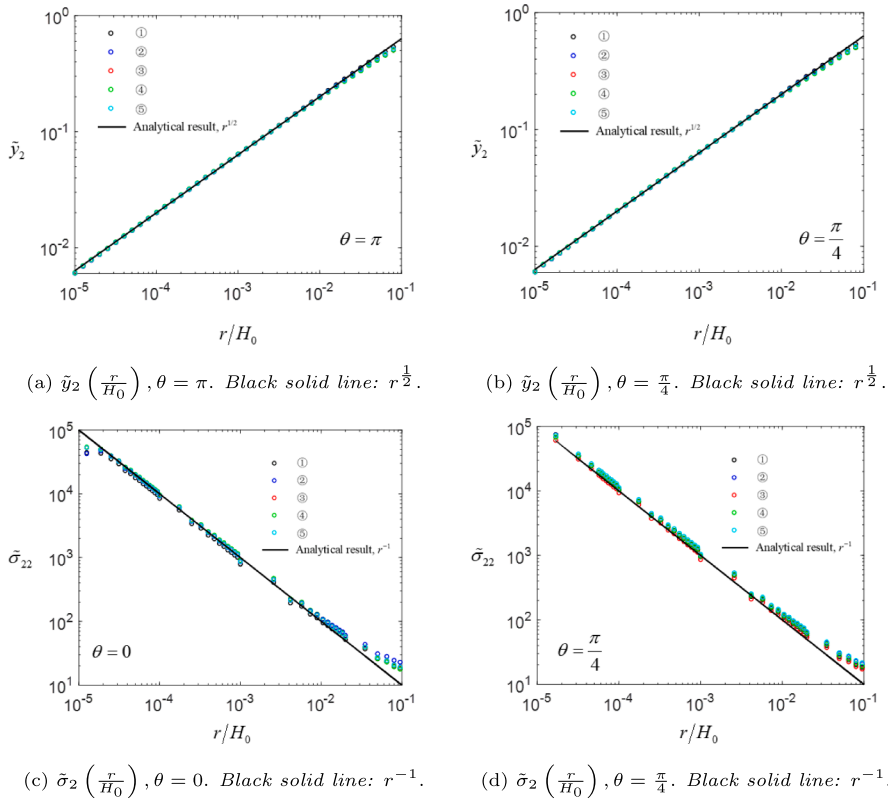

(a) $\tilde{y}_2\left(\frac{r}{H_0}\right), \theta = \pi$. *Black solid line:* $r^{\frac{1}{2}}$. (b) $\tilde{y}_2\left(\frac{r}{H_0}\right), \theta = \frac{\pi}{4}$. *Black solid line:* $r^{\frac{1}{2}}$.

(c) $\tilde{\sigma}_2\left(\frac{r}{H_0}\right), \theta = 0$. *Black solid line:* r^{-1}. (d) $\tilde{\sigma}_2\left(\frac{r}{H_0}\right), \theta = \frac{\pi}{4}$. *Black solid line:* r^{-1}.

Fig. 9. Radial behavior of scaled deformation $\tilde{y}_2$ (Eq. (45)) and scaled Cauchy stress component $\tilde{\sigma}_{22}$ (Eq. (46)).

introduced in [1–3] and use the crack tip integrals developed in [4,5] to evaluate the coefficients of the asymptotic expansion of the elastic fields at the crack tip. It is observed that the canonical transformation of the asymptotic boundary value problem maps the general anisotropic case to the isotropic problem [42].

Several cases of discrete and continuous distributions of fibers are considered and good agreement is always found between the numerical results and the analytical predictions. Given its use in the experimental literature, the *von Mises* distribution is analyzed in detail and conditions for a pure Mode I crack are found and discussed. It is then observed that specific distributions of orientations correspond to an isotropic material response in the region of dominance of the asymptotic fields, which we call conditions of *asymptotic isotropy*. Mathematically, it corresponds to the fact that the asymptotic boundary value problem becomes identical to the isotropic case [42] *without* resorting to the canonical transformation. A set of discrete and continuous distributions are found to obey the conditions of *asymptotic isotropy*. Numerical analysis of the asymptotic elastic fields confirms the theoretical predictions. Finally, it is shown that the canonical transformation of the asymptotic boundary value problem can be interpreted as an *asymptotic universal one-to-one mapping* between anisotropic and isotropic Neo-Hookean thin sheets under conditions of plane stress.

CRediT authorship contribution statement

Luca Di Stasioa: Conceptualization, Data curation, Formal analysis, Methodology, Visualization, Writing - original draft, Writing - review & editing. **Yin Liua:** Conceptualization, Data curation, Formal analysis, Methodology, Software, Validation, Visualization, Writing - review & editing. **Brian Morana:** Conceptualization, Data curation, Formal analysis, Methodology, Funding acquisition, Project administration, Resources, Supervision, Writing - review & editing.

Declaration of Competing Interest

The authors declare that they have no known competing financial interests or personal relationships that could have appeared to influence the work reported in this paper.

References

[1] Z. Guo, X. Peng, B. Moran, A composites-based hyperelastic constitutive model for soft tissue with application to the human annulus fibrosus, J. Mech. Phys. Solids 54 (9) (2006) 1952–1971, https://doi.org/10.1016/j.jmps.2006.02.006.
[2] Z. Guo, X. Peng, B. Moran, Mechanical response of neo-hookean fiber reinforced incompressible nonlinearly elastic solids, Int. J. Solids Struct. 44 (6) (2007) 1949–1969, https://doi.org/10.1016/j.ijsolstr.2006.08.018.
[3] Z. Guo, X. Peng, B. Moran, Large deformation response of a hyperelastic fibre reinforced composite: Theoretical model and numerical validation, Compos. A Appl. Sci. Manuf. 38 (8) (2007) 1842–1851, https://doi.org/10.1016/j.compositesa.2007.04.004.
[4] Y. Liu, B. Moran, Asymptotic path-independent integrals for the evaluation of crack-tip parameters in a neo-hookean material, Int. J. Fract. 224 (2020) 133–150, https://doi.org/10.1007/s10704-020-00452-4.
[5] Y. Liu, B. Moran, Large deformation near a crack tip in a fiber-reinforced neo-hookean sheet, J. Mech. Phys. Solids 143 (2020) 104049, https://doi.org/10.1016/j.jmps.2020.104049.
[6] S. Federico, W. Herzog, Towards an analytical model of soft biological tissues, J. Biomech. 41 (16) (2008) 3309–3313, https://doi.org/10.1016/j.jbiomech.2008.05.039.
[7] K.M. Meek, T. Blamires, G.F. Elliott, T.J. Gyi, C. Nave, The organisation of collagen fibrils in the human corneal stroma: A synchrotron x-ray diffraction study, Curr. Eye Res. 6 (7) (1987) 841–846, https://doi.org/10.3109/02713688709034853.
[8] P.B. Canham, H.M. Finlay, J.A. Kiernan, G.G. Ferguson, Layered structure of saccular aneurysms assessed by collagen birefringence, Neurol. Res. 21 (7) (1999) 618–626, https://doi.org/10.1080/01616412.1999.11740986.
[9] H.M. Finlay, L. McCullough, P.B. Canham, Three-dimensional collagen organization of human brain arteries at different transmural pressures, J. Vasc. Res. 32 (5) (1995) 301–312, https://doi.org/10.1159/000159104.
[10] J.-L. Gennisson, T. Deffieux, E. Macé, G. Montaldo, M. Fink, M. Tanter, Viscoelastic and anisotropic mechanical properties of in vivo muscle tissue assessed by supersonic shear imaging, Ultrasound Med. Biol. 36 (5) (2010) 789–801, https://doi.org/10.1016/j.ultrasmedbio.2010.02.013.

[11] S. Sherifova, G.A. Holzapfel, Biomechanics of aortic wall failure with a focus on dissection and aneurysm: A review, Acta Biomater. 99 (2019) 1–17, https://doi.org/10.1016/j.actbio.2019.08.017. doi: 10.1016/j.actbio.2019.08.017.
[12] A.D. Freed, D.R. Einstein, I. Vesely, Invariant formulation for dispersed transverse isotropy in aortic heart valves, Biomech. Model. Mechanobiol. 4 (2–3) (2005) 100–117, https://doi.org/10.1007/s10237-005-0069-8.
[13] T. Nakajima, T. Kurokawa, S. Ahmed, W. Li Wu, J.P. Gong, Characterization of internal fracture process of double network hydrogels under uniaxial elongation, Soft Matter 9 (6) (2013) 1955–1966, https://doi.org/10.1039/c2sm27232f.
[14] J.A. Stella, A. D'Amore, W.R. Wagner, M.S. Sacks, On the biomechanical function of scaffolds for engineering load-bearing soft tissues, Acta Biomater. 6 (7) (2010) 2365–2381, https://doi.org/10.1016/j.actbio.2010.01.001.
[15] A.S. Gladman, E.A. Matsumoto, R.G. Nuzzo, L. Mahadevan, J.A. Lewis, Biomimetic 4d printing, Nat. Mater. 15 (4) (2016) 413–418, https://doi.org/10.1038/nmat4544.
[16] T.C. Gasser, R.W. Ogden, G.A. Holzapfel, Hyperelastic modelling of arterial layers with distributed collagen fibre orientations, J. R. Soc. Interface 3 (6) (2005) 15–35, https://doi.org/10.1098/rsif.2005.0073.
[17] P. J. Flory, Thermodynamic relations for high elastic materials, Transactions of the Faraday Society 57 829. doi:10.1039/tf9615700829.
[18] R. Ogden, Nearly isochoric elastic deformations: Application to rubberlike solids, J. Mech. Phys. Solids 26 (1) (1978) 37–57, https://doi.org/10.1016/0022-5096(78)90012-1.
[19] J. Simo, R. Taylor, K. Pister, Variational and projection methods for the volume constraint in finite deformation elasto-plasticity, Comput. Methods Appl. Mech. Eng. 51 (1–3) (1985) 177–208, https://doi.org/10.1016/0045-7825(85)90033-7.
[20] C. Sansour, On the physical assumptions underlying the volumetric-isochoric split and the case of anisotropy, Eur. J. Mech. A. Solids 27 (1) (2008) 28–39, https://doi.org/10.1016/j.euromechsol.2007.04.001.
[21] S. Federico, T.C. Gasser, Nonlinear elasticity of biological tissues with statistical fibre orientation, J. R. Soc. Interface 7 (47) (2010) 955–966, https://doi.org/10.1098/rsif.2009.0502.
[22] Y. Lanir, Constitutive equations for fibrous connective tissues, J. Biomech. 16 (1) (1983) 1–12, https://doi.org/10.1016/0021-9290(83)90041-6.
[23] G.A. Holzapfel, R.W. Ogden, Constitutive modelling of arteries, Proc. Roy. Soc. A: Mathe., Phys. Eng. Sci. 466 (2118) (2010) 1551–1597, https://doi.org/10.1098/rspa.2010.0058.
[24] G. Chagnon, M. Rebouah, D. Favier, Hyperelastic energy densities for soft biological tissues: A review, J. Elast. 120 (2) (2014) 129–160, https://doi.org/10.1007/s10659-014-9508-z.
[25] G.A. Holzapfel, R.W. Ogden, S. Sherifova, On fibre dispersion modelling of soft biological tissues: a review, Proc. Roy. Soc. A: Mathe., Phys. Eng. Sci. 475 (2224) (2019) 20180736, https://doi.org/10.1098/rspa.2018.0736.
[26] K. Volokh, Modeling failure of soft anisotropic materials with application to arteries, J. Mech. Behav. Biomed. Mater. 4 (8) (2011) 1582–1594, https://doi.org/10.1016/j.jmbbm.2011.01.002.
[27] K. Volokh, Prediction of arterial failure based on a microstructural bi-layer fiber–matrix model with softening, J. Biomech. 41 (2) (2008) 447–453, https://doi.org/10.1016/j.jbiomech.2007.08.001.
[28] T.C. Gasser, An irreversible constitutive model for fibrous soft biological tissue: A 3-d microfiber approach with demonstrative application to abdominal aortic aneurysms, Acta Biomater. 7 (6) (2011) 2457–2466, https://doi.org/10.1016/j.actbio.2011.02.015.
[29] D. Li, A.M. Robertson, G. Lin, M. Lovell, Finite element modeling of cerebral angioplasty using a structural multi-mechanism anisotropic damage model, Int. J. Numer. Meth. Eng. 92 (5) (2012) 457–474, https://doi.org/10.1002/nme.4342.
[30] A. Ferrara, A. Pandolfi, Numerical modelling of fracture in human arteries, Comput. Methods Biomech. Biomed. Eng. 11 (5) (2008) 553–567, https://doi.org/10.1080/10255840701771743.
[31] E. Peña, J.A. Peña, M. Doblaré, On the mullins effect and hysteresis of fibered biological materials: A comparison between continuous and discontinuous damage models, Int. J. Solids Struct. 46 (7–8) (2009) 1727–1735, https://doi.org/10.1016/j.ijsolstr.2008.12.015.
[32] D. Balzani, S. Brinkhues, G.A. Holzapfel, Constitutive framework for the modeling of damage in collagenous soft tissues with application to arterial walls, Comput. Methods Appl. Mech. Eng. 213–216 (2012) 139–151, https://doi.org/10.1016/j.cma.2011.11.015.
[33] E. Maher, A. Creane, C. Lally, D.J. Kelly, An anisotropic inelastic constitutive model to describe stress softening and permanent deformation in arterial tissue, J. Mech. Behav. Biomed. Mater. 12 (2012) 9–19, https://doi.org/10.1016/j.jmbbm.2012.03.001.
[34] T. Schmidt, D. Balzani, G.A. Holzapfel, Statistical approach for a continuum description of damage evolution in soft collagenous tissues, Comput. Methods Appl. Mech. Eng. 278 (2014) 41–61, https://doi.org/10.1016/j.cma.2014.04.011.
[35] R.J. Nims, K.M. Durney, A.D. Cigan, A. Dusséaux, C.T. Hung, G.A. Ateshian, Continuum theory of fibrous tissue damage mechanics using bond kinetics: application to cartilage tissue engineering, Interface Focus 6 (1) (2016) 20150063, https://doi.org/10.1098/rsfs.2015.0063.
[36] O. Gültekin, S.P. Hager, H. Dal, G.A. Holzapfel, Computational modeling of progressive damage and rupture in fibrous biological tissues: application to aortic dissection, Biomech. Model. Mechanobiol. 18 (6) (2019) 1607–1628, https://doi.org/10.1007/s10237-019-01164-y.
[37] W. Li, Damage models for soft tissues: A survey, J. Med. Biol. Eng. 36 (3) (2016) 285–307, https://doi.org/10.1007/s40846-016-0132-1.
[38] A.J.M. Spencer (Ed.), Continuum Theory of the Mechanics of Fibre-Reinforced Composites, Springer Vienna, 1984. doi:10.1007/978-3-7091-4336-0.
[39] J.A. Rogers, T. Someya, Y. Huang, Materials and mechanics for stretchable electronics, Science 327 (5973) (2010) 1603–1607, https://doi.org/10.1126/science.1182383.
[40] S. Lin, H. Yuk, T. Zhang, G.A. Parada, H. Koo, C. Yu, X. Zhao, Stretchable hydrogel electronics and devices, Adv. Mater. 28 (22) (2015) 4497–4505, https://doi.org/10.1002/adma.201504152.
[41] C. Yang, Z. Suo, Hydrogel ionotronics, Nat. Rev. Mater. 3 (6) (2018) 125–142, https://doi.org/10.1038/s41578-018-0018-7.
[42] J.K. Knowles, E. Sternberg, Large deformations near a tip of an interface-crack between two neo-hookean sheets, J. Elast. 13 (3) (1983) 257–293, https://doi.org/10.1007/bf00042997.
[43] F.S. Wong, R.T. Shield, Large plane deformations of thin elastic sheets of neo-hookean material, Zeitschrift für angewandte Mathematik und Physik ZAMP 20 (2) (1969) 176–199, https://doi.org/10.1007/BF01595559.
[44] G. Sih, P. Paris, G. Irwin, On cracks in rectilinearly anisotropic bodies, Int. J. Fracture Mech. 1 (3) (1965), https://doi.org/10.1007/bf00186854.
[45] J. Chang, J. Li, Evaluation of asymptotic stress field around a crack tip for neo–hookean hyperelastic materials, Int. J. Eng. Sci. 42 (15–16) (2004) 1675–1692, https://doi.org/10.1016/j.ijengsci.2004.03.009.
[46] C. Frank, B. MacFarlane, P. Edwards, R. Rangayyan, Z.-Q. Liu, S. Walsh, R. Bray, A quantitative analysis of matrix alignment in ligament scars: A comparison of movement versus immobilization in an immature rabbit model, J. Orthop. Res. 9 (2) (1991) 219–227, https://doi.org/10.1002/jor.1100090210.
[47] C. Frank, D. McDonald, D. Bray, R. Bray, R. Rangayyan, D. Chimich, N. Shrive, Collagen fibril diameters in the healing adult rabbit medial collateral ligament, Connect. Tissue Res. 27 (4) (1992) 251–263, https://doi.org/10.3109/03008209209007000.
[48] C. Hurschler, B. Loitz-Ramage, R. Vanderby, A structurally based stress-stretch relationship for tendon and ligament, J. Biomech. Eng. 119 (4) (1997) 392–399, https://doi.org/10.1115/1.2798284.
[49] M.S. Sacks, D.B. Smith, E.D. Hiester, The aortic valve microstructure: Effects of transvalvular pressure, J. Biomed. Mater. Res. 41 (1) (1998) 131–141, https://doi.org/10.1002/(sici)1097-4636(199807)41:1<131::aid-jbm16>3.0.co;2-q.
[50] M.S. Sacks, Incorporation of experimentally-derived fiber orientation into a structural constitutive model for planar collagenous tissues, J. Biomech. Eng. 125 (2) (2003) 280–287, https://doi.org/10.1115/1.1544508.
[51] M. Landuyt, G. A. Holzapfel, P. Verdonck, Structural quantification of collagen fibers in abdominal aortic aneurysms , Master's thesis, Department of Solid Mechanics, Royal Institute of Technology in Stockholm and Department of Civil Engineering, Ghent University, Master Thesis in electromechanical engineering, option biomedical engineering. 2006. URL https://lib.ugent.be/catalog/rug01:001311703.
[52] R.D. Rosenkrantz (Ed.), E.T. Jaynes: Papers on Probability, Statistics and Statistical Physics, Springer Netherlands, 1983. doi:10.1007/978-94-009-6581-2.
[53] N.I. Fisher, Statistical Analysis of Circular Data, Cambridge University Press, 1993. doi:10.1017/cbo9780511564345.
[54] K.L. Billiar, M.S. Sacks, Biaxial mechanical properties of the native and glutaraldehyde-treated aortic valve cusp: Part II—a structural constitutive model, J. Biomech. Eng. 122 (4) (2000) 327–335, https://doi.org/10.1115/1.1287158.
[55] J.A. Holdener, Math bite: Sums of sines and cosines, 126–126, Math. Mag. 82 (2) (2009), https://doi.org/10.1080/0025570x.2009.11953606.
[56] M.P. Knapp, Sines and cosines of angles in arithmetic progression, Math. Mag. 82 (5) (2009) 371–372, https://doi.org/10.4169/002557009x478436.